Femtosecond-Laser Microstructuring of Ribs on Active (Yb,Nb):RTP/RTP Planar Waveguides

J. Cugat, A. Ruiz de la Cruz, R. Solé, A. Ferrer, J. J. Carvajal, X. Mateos, J. Massons, J. Solís, G. Lifante, F. Díaz, and M. Aguiló

***Abstract*—We have produced rib waveguides by femtosecond-laser structuring of active (Yb,Nb):$RbTiOPO_4$/$RbTiOPO_4$ epitaxial layers. The ribs were produced by the approximation scanning technique combined with beam multiplexing. The so-obtained waveguides are trapezoidal in shape and show propagation losses with an upper bound of $\sim$4 dB/cm. A simulation of the rib waveguides with real geometry parameters reveals high levels of light confinement at 632 and 972 nm. The near-field patterns of the fundamental modes have been obtained by exciting the waveguides at wavelengths of 632 and 972 nm. Micro-Raman spectroscopy study reveals that the damage to the crystalline structure in the rib boundaries, showing no amorphization traces, is around 3 μm in length and depth, which is significantly shorter than the total width of the ribs.**

***Index Terms*—Femtosecond-laser microstructuring, nonlinear optical crystals, waveguides.**

I. Introduction

$RbTiOPO_4$ (RTP) belongs to the $KTiOPO_4$ (KTP) family of nonlinear optical crystals. It crystallizes in the orthorhombic space group $Pna2_1$ [1]. Because of its non-linear optical properties, RTP can be used for frequency doubling the light emitted by Yb and Nd lasers with a wavelength close to 1 μm [2]. RTP can also be doped with active ions to obtain a self-frequency doubling (SFD) material, which can be useful for compact and efficient laser sources in the visible range. KTP family of non-linear optical crystals has large electro-optical coefficients and low dielectric constants making them attractive for such electro-optical applications as modulators and Q switches [3]. These interesting properties make RTP a good candidate as a base material for integrated photonics.

Among other possible active ions, Yb^{3+} was chosen for this study because it has several advantages. Its ionic radius is much closer to the radius of Ti^{4+} than the ionic radius of the other Ln^{3+} ions, which produces a higher distribution coefficient of Yb^{3+} in the crystals of the KTP family [4]. The emission wavelength of Yb^{3+} is similar to that of Nd^{3+} in the region close to 1 μm, but its energy scheme is simpler. It has only two energy levels: the ground state $^2F_{7/2}$ and the exited state $^2F_{5/2}$. This prevents some effects that reduce the laser efficiency, for instance, excited-state absorption, cross-relaxation, and upconversion. On the other hand, the similarity between the pumping and the laser wavelength means that there is a small quantum defect that reduces the thermal loading of the crystals during laser operation [5]. Yb^{3+} also has no absorption losses at the second harmonic generation (SHG) frequency, which makes it particularly suitable for SFD [6].

The maximum doping levels of Yb^{3+} previously achieved in KTP bulk crystals are not enough for laser operation. The distribution coefficient of Yb^{3+} in single-doped RTP is slightly higher than in KTP but not enough for lasing [4]. The codoping of RTP with Yb^{3+} and Nb^{5+} significantly increases the distribution coefficient of Yb^{3+} in RTP [7]. Thus, the content of Yb^{3+} in RTP was high enough to successfully obtain laser emission in these crystals [8].

In order to avoid the difficulties of growing bulk (Yb,Nb):RTP crystals, which are often of low quality [9], and to increase the optical path, (Yb,Nb):RTP planar waveguides were grown on RTP substrates by the liquid phase epitaxy (LPE) method [10]. In these samples efficient type II SHG has already been reported [11].

For the fabrication of nonlinear optical waveguides, ion-incorporation techniques such as ion implantation [12] and ion diffusion have been applied [3]. Other techniques such as LPE [10], molecular beam epitaxy [13], chemical vapor deposition, and pulsed laser deposition [14] have also been widely used to obtain optical waveguides. Subsequent structuring methods such as ion milling [15] reactive ion etching, [16], and laser structuring, [17] are also available.

Microstructuring the surface by femtosecond-laser (fs-laser) ablation could be a good technique for the commercial fabrication of optical waveguides in the field of integrated photonics. The main advantage it has over other techniques is that it enables rapid prototyping with a relatively cheaper production cost that does not require to be carried out in a clean room.

Manuscript received September 04, 2012; revised November 22, 2012; accepted November 23, 2012. Date of publication November 29, 2012; date of current version December 31, 2012. This work was supported by the Spanish Government under Projects TEC2010-21574-C02-02, TEC2011-22422, MAT2011-29255-C02-02, PI09/90527, and the Catalan Authority under Project 2009SGR235. This work was also supported in part by the European Commission under the Seventh Framework Programme under Project FP7-SPACE-2010-1-GA-263044. The work of J. Cugat was supported by the Spanish Government under the FPI fellowship BES-2009-024190.

J. Cugat, R. Solé, J. J. Carvajal, X. Mateos, J. Massons, F. Díaz, and M. Aguiló are with Física i Cristal.logafía de Materials i Nanomaterials, Universitat Rovira i Virgili, 43007 Tarragona, Spain (e-mail: jaume.cugat@urv.cat; rosam.sole@urv.cat; joanjosep.carvajal@urv.cat; xavier.mateos@urv.cat; jaume.masons@urv.cat; magdalena.aguilo@urv.cat).

A. Ruiz de la Cruz and J. Solís, are with Laser Processing Group, Instituto de Óptica, 28006 Madrid, Spain (e-mail: alejandro@io.cfmac.csic.es; j.solis@io.cfmac.csic.es).

A. Ferrer was with the Laser Processing Group, Instituto de Óptica, 28006 Madrid, Spain. He is now with the Ultrafast Dynamics Group, Institute for Quantum Electronics, ETH Zurich, CH-8093 Zurich, Switzerland (e-mail: a.ferrer@io.cfmac.csic.es).

G. Lifante is with Departamento de Física de Materiales C-IV, Universidad Autónoma de Madrid, 28049 Madrid, Spain (e-mail: gines.lifante@uam.es).

Color versions of one or more of the figures in this paper are available online at http://ieeexplore.ieee.org.

Digital Object Identifier 10.1109/JLT.2012.2230615

In this paper, we show that low-loss rib waveguides can be produced by fs-laser structuring on (Yb,Nb):RTP epitaxial layers grown by LPE. The microstructures were generated by fs-laser ablation. A morphological, optical, and Raman spectroscopy characterization of the ribs is presented.

II. Rib Waveguide Fabrication

A. Structure Performance Simulations

In order to determine what the best geometry is for the ribs in terms of light confinement, the performance of the devised structures at 632 and 972 nm were simulated using the MG finite difference (Real) method at 632 and 972 nm from the OlympIOs software package.

The initial structure considered is an epitaxial layer (Yb, Nb):RTP with thickness of 10 μm on bulk RTP (see Section II-B). Since the ribs are produced by sculpting two parallel trenches on the sample surface by laser surface structuring, the initial simulations considered ribs of different widths and heights using the previously determined values of the corresponding refractive indexes of the epilayer and the substrate.

The real refractive indexes of the waveguide and the substrate in TM polarization were 1.8967 for the layer and 1.8897 for the substrate at 632 nm [9]. Similar measurements were made in TM polarization at 972 nm and the values obtained for the refractive indexes were 1.8632 for the layer and 1.8573 for the substrate, measured in this study.

The rib structures considered in the initial simulation were 8 μm height and 6–18 μm wide (with 2 μm steps). The depth was chosen to be 8 μm, because the initial tests of fs-laser structuring on RTP substrates showed this value to provide a good compromise in terms of crystal damage and groove shape. The confinement area for simulation was designed taking into account the rib boundary that extended down to the planar waveguide–substrate interface. The simulation enables to estimate approximately the percentage of energy confined within this region (confinement). Although part of the mode propagates through the planar region, the simulation reveals a high level of confinement. The estimated confinement values depended on rib dimensions and were in all the cases above 99.0 % at both 632 and 972 nm. The experimentally determined losses were analyzed by simulating the power attenuation in the waveguides using the beam propagation method.

B. Growth by LPE

We grew epitaxial layers of (Yb,Nb):RTP on (001) RTP substrates. Plates perpendicular to the *c* crystallographic direction and cut from RTP single crystals were used as substrates. The *ab* plane is interesting because it contains the type II noncritical phase matching SHG directions for the range between 985 and 1118 nm. This range contains the Yb^{3+} laser emission at 1060 nm.

The epitaxial layers were grown by the LPE method from WO_3-containing solutions. Rb_2CO_3 (99%), $NH_4H_2PO_4$ (99%), TiO_2 (99.9%), Yb_2O_3 (99.9%), Nb_2O_5 (99.9%), and WO_3 (99.9%) were used as starting chemicals. The procedure was similar to that already reported Solé and coworkers for the

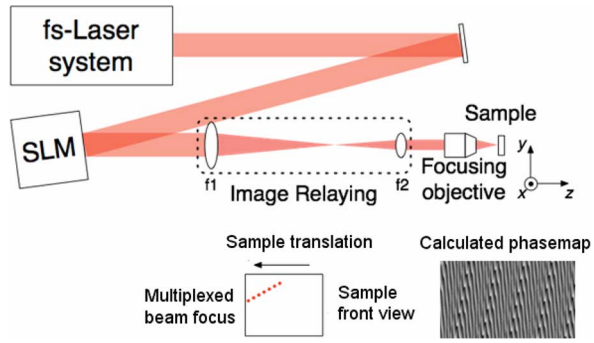

Fig. 1. Experimental setup used to inscribe the surface channels for the fabrication of waveguides. The focused beam is multiplexed into seven spots, which makes it possible to perform the approximation scanning technique in a single scan.

LPE growth of several epitaxial layers [18], [19]. The solution composition was Rb_2O-P_2O_5-TiO_2-Yb_2O_3-Nb_2O_5-WO_3 = 43.90-23.60-20.70-1.35-0.45-10 (mol%). To start the growth process, the solution was supersaturated by decreasing its temperature by 2 K below the saturation temperature, which was around 1153 K. In all the LPE experiments, a rotation of 60 r/min was applied. The epitaxial layers grown showed good optical quality and the average growth rate was 8.3 μm/h. The chemical composition of the epitaxies was determined by electron probe microanalysis and the result was $RbTi_{0.958}Yb_{0.016}Nb_{0.026}OPO_4$. The thickness of the as-grown epitaxial layers measured by interferometric microscopy and using the substrate surface as a reference was around 50 μm. After growth, the epitaxial layer was polished up to 10 μm in thickness.

C. Femtosecond-Laser Setup and Experimental Conditions

In order to produce the rib structures, sets of two parallel ablated channels were micromachined on the sample surface using the fs-laser irradiation setup sketched in Fig. 1. We used a pulsed fs-laser amplification system (Tsunami and Spitfire from Spectra-Physics), working at a 1 KHz repetition rate and a pulse duration of $\tau_p \approx 120$ fs. The output pulse energy was $E = 1$ mJ and the central wavelength $\lambda = 799$ nm. We also used a spatial light modulator (SLM, Hamamatsu X8267) to control the beam wavefront before focusing on the surface of the sample. This allowed us to design the intensity profile of the focused beam. An image relaying system with magnification $M = 0.4$ (f1 = 50 cm and f2 = 20 cm) transferred the beam at the SLM surface to the back-focal position of the focusing microscope objective (Mitutoyo M Plan Apo NIR 20X NA = 0.4). The sample was placed on a three-axis motorized stage. During processing, the sample was translated at a speed of v = 100 μm/s.

In order to improve the quality of the micromachined channels, we used the *approximation scanning* technique [20]. It consists of performing several irradiation scans, each one slightly displaced from the previous one in the direction perpendicular to the channels. This produces steeper channel walls than when a single irradiation scan is used. It also helps minimizing the redeposition of debris in the walls of the channel and reduce surface roughness.

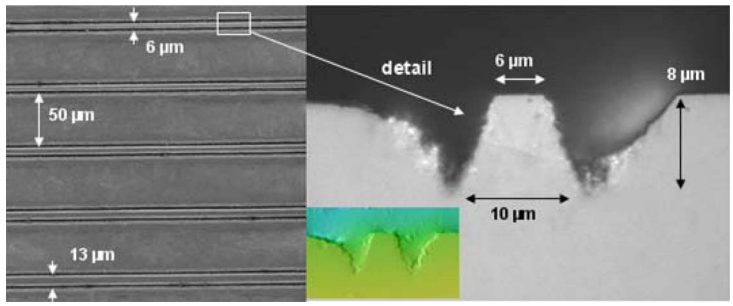

Fig. 2. (Left) General view of the rib waveguides produced obtained with an ESEM. (Right) Cross-sectional view of a rib with 6 μm width at the top and 10 μm at the bottom. The inset shows the same region imaged with an optical confocal microscope.

Our approach uses an SLM to multiplex the irradiation beam at the material surface, creating seven spots. The spots are arranged diagonally (see Fig. 1), such that each spot rewrites the channel written by the previous one, but with a slight lateral displacement just as the approximation scanning does. Thus, a multiplexed beam requires only a single scan to inscribe a channel in the sample, while a nonmultiplexed beam requires several scans. In order to multiplex the beam, the wavefront of the irradiation was tailored using the phase-only SLM in order to obtain a predesigned intensity distribution at the focus of the lens. The corresponding phase map is shown in Fig. 1. It was generated using a weighted Gerchberg–Saxton algorithm, which helps to equalize the peak intensities of the multiplexed spots in the designed intensity distribution [21].

During the channel structuring process, the value of the local maximum fluence of each multiplexed spot (2.1 μm full-width at half-maximum) at the surface was 4.1 J/cm^2 (per pulse). For the scanning speed used, a multiplexed spot receives in average of 21 pulses. For reference, the single-shot/single-spot ablation threshold of the sample is 1.1 J/cm^2. It is worth noting at this point that the sample shows a negligible linear absorption at the irradiation wavelength, and therefore, surface ablation is the consequence of multiphoton and avalanche ionization processes associated to the high peak power of fs-laser pulses [22].

III. Rib Waveguide Characterization

A. Environmental Scanning Electron Microscopy and Confocal Morphological Characterization

Fig. 2 shows an environmental scanning electron microscopy (ESEM) image of the ribs made on the planar waveguides, obtained using a Quanta 200 microscope. After polishing the end face of the sample, which is perpendicular to the ribs, images of some channels were obtained both with the ESEM and a confocal microscope, as can be seen in the detail of Fig. 2 (right). These images reveal that, in terms of visual roughness, the rib had a good shape. In this figure, it can be seen that the internal groove wall, that is to say, the rib wall, shows clearly less roughness than the external groove wall. The rms roughness of the rib walls is $\sim$500 nm, an encouraging result if it is taken into account that this value is $\sim$50% of the wavelength of interest (around 1 μm). This confirms that the use of *approximation scanning* combined with the beam multiplexing is beneficial for the performance of the laser written structures.

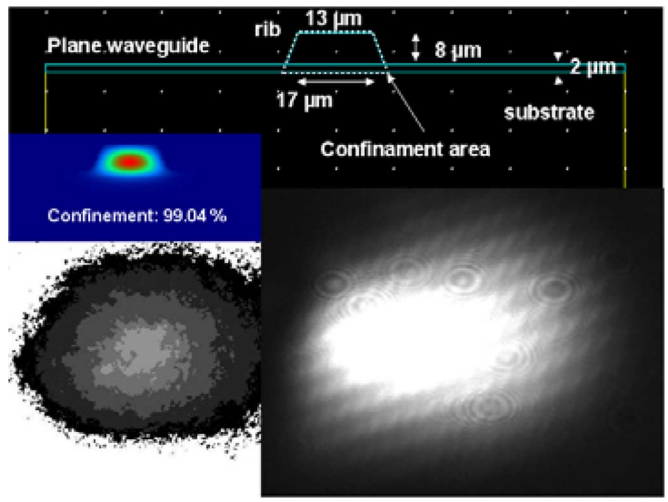

Fig. 3. CCD picture of the near field pattern of the mode obtained at 972 nm and intensity profile. Geometry of the rib used for simulation and confinement obtained by simulation.

Still, the shape of the rib was not rectangular but trapezoidal. The produced grooves were $\sim$8 μm deep. At the top, the dimensions of the channels produced were 6, 7, 8, 9, 13, 14, 15, and 18 μm. The rib walls show a slope $\mathrm{tg}(\alpha) \sim 0.25(\sim 14^\circ)$. This makes, as can be seen in Fig. 2, that the bases of the ribs are about 4 μm wider than their tops while the structures are symmetrical in all the cases. The observed trapezoidal shape does not imply though a big problem in terms of confinement, as shown by the simulations with real parameters.

B. Near-Field Pattern and Propagation Losses

As shown in Fig. 2, the walls of the ribs obtained by fs-laser structuring are not vertical. It was thus advisable to perform a simulation with real parameters. The simulations were carried out with the same software that was used in the preliminary simulation. As above mentioned, the ribs obtained are trapezoidal in shape. They were 6–18 μm at the top, and 10–22 μm at the base and they were all symmetrical. The simulation again reveals a high confinement. The confinement values provided by numerical simulations ranged between 99.75% and 99.80% at 632 nm and between 98.37% and 99.04% at 972 nm. So, theoretically the confinement is high even for the rib with the lowest cross section area.

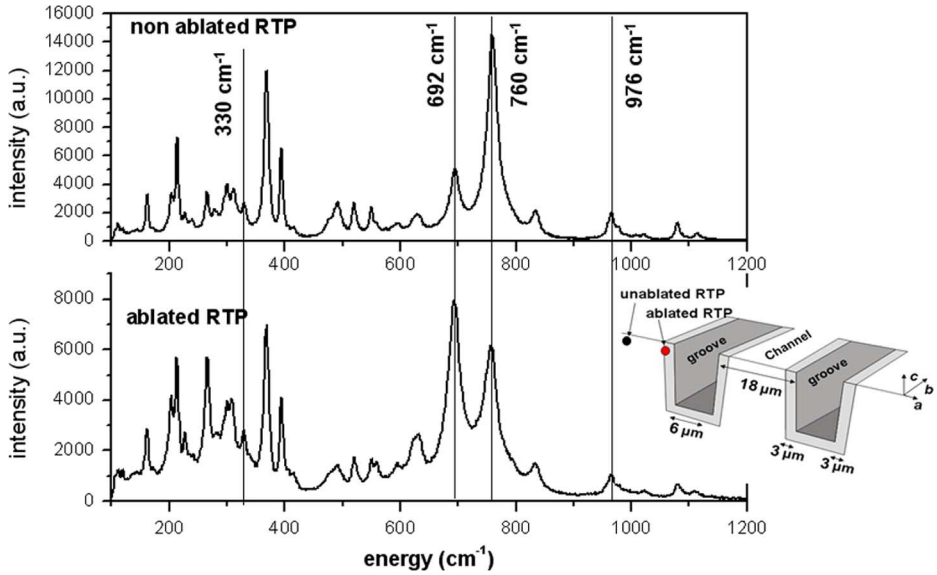

Fig. 4. Raman spectra of the ablated and unablated RTP zones. Inset: scheme of a channel with the indications of the points where the Raman spectra were taken.

The rib waveguide modes were excited at 632 and 972 nm in order to test the performance of the laser-written structures. All the channels were excited successfully but the 13 μm channel (width at the top) was used for characterization. As an example, Fig. 3 shows the near field pattern of this channel at a wavelength of 972 nm. A high optical density filter was used to record the mode's profile with a CCD camera. The propagation losses of the rib waveguide with a top width of the 6 μm were estimated at 972 nm by coupling a laser beam to the waveguide with a 10 $\times$ objective microscope. The fundamental waveguide mode was excited using an *xyz* translation stage in order to prevent the multi modal dispersion. The light transmitted by the waveguide was then collected using a 50$\times$ objective microscope. The power of the laser beam was measured before the input objective microscope and after the output one. The optical losses of these rib waveguides were evaluated by single pass transmission measurements. The expression used in dB/cm was $\mathrm{Loss} = (10/d)\log(P_{\mathrm{out}}/P_{\mathrm{in}})$, where d is the length of the channel waveguides. Some corrections had to be made to both powers (P_{out} and P_{in}). The estimation of the propagation losses has to consider though some corrections to the values of P_{out} and P_{in} like the transmission losses of the microscope objectives, the Fresnel losses at the waveguide interfaces, the losses associated to the mismatch between the laser field distribution at the focal plane of the lens and the mode of the waveguide (calculated through the corresponding overlapping integral [23]). Since we have not corrected the losses associated to the effect of the different numerical apertures of the waveguide and the input microscope objective and the losses associated to the absorption of the beam by the small amount of Yb present in the waveguide, the estimated value of the propagation loss have to be considered as an exaggerated upper bound. The upper limit obtained is 4.4 dB/cm which compares well with recent values obtained by fs-laser structuring of Nd:GGG [24]. In this respect, it is worth noting that BPM simulations of the propagation loss of this waveguide using a roughness with a rms value of 500 nm provide values in the order of 7 dB/cm which indicate that the "visual" estimation of roughness above indicated should be overestimated. The roughness was modeled via a seventh order autoregressive estimator calculated using the measured roughness function $f(z)$. In our case, this function indicates that the underlying statistics are exponential and the corresponding autocorrelation function gives a standard deviation of $\sigma = 0.21$ μm and a correlation length of $Lc = 0.78$ μm.

C. Micro-Raman Scattering

One of the techniques used to investigate the induced microscale modifications in the crystalline material is micro-Raman (μ-Raman) measurement [25]. Micro-Raman scattering measurements were made using a micro-Raman Reinshaw Confocal InVia spectrometer equipped with a Leica 2500 confocal microscope and a CCD camera as the detector. With this equipment, 64 consecutive Raman spectra were recorded on the surface of the sample, at 1 μm intervals. The excitation wavelength for these measurements was 514 nm. The Raman signal was collected using a pinhole and focusing every time on the desired region.

As can be seen in Fig. 4, the Raman spectrum for these materials is very complex: it has more than 30 peaks corresponding to A_1, A_2, B_1, and B_2 symmetry representations [25]. We observed that all the peaks in the unablated area are also present in the ablated area, indicating that femtosecond irradiation does not induce amorphisation of (Yb,Nb):RTP, at least in the spatial resolution we used.

In general, we observed that the intensity of the peaks in the ablated area of the sample is less than the intensity of the peaks for the unablated area. The intensity of the Raman peaks is a function of the change in polarization of the molecule during a vibration. Thus, a significant decrease in intensity of the bands indicates a constraint on the vibrational degrees of freedom of the molecule [26]. This constraint on the vibrational degrees of freedom of the molecule is due to the introduction of defects and changes in the crystallographic structure of the material.

Basically, the Raman spectra recorded correspond to those of RTP in a $z(yy)\bar{z}$ polarization configuration [27]. However, we observed significant differences in the intensity of the peaks located at $\sim$692 and $\sim$760 cm^{-1} for the spectra recorded in the ablated and unablated areas, respectively. While the first peak increases its intensity considerably in the ablated zone, the intensity of the peak at 760 cm^{-1} decreases considerably in the same zone. The $\sim$760 cm^{-1} signal corresponds to the ν_2 vibration mode of the TiO_6 octahedron, and it is the most intense peak for the polarized $z(yy)\bar{z}$ Raman spectrum of RTP. The $\sim$692 cm^{-1} signal is also related to the ν_2 vibration mode of the TiO_6 octahedron in the same polarized configuration, but its intensity is considerably lower than the one at 760 cm^{-1}. However, it may also be related to ν_1 and ν_3 vibration modes of the TiO_6 octahedron in the $x(yz)\bar{x}$, $y(xx)\bar{y}$, and $y(zz)\bar{y}$ polarization configurations, where it corresponds to the most intense peak of these spectra. Thus, the difference in intensity of these peaks in the ablated region spectrum compared with the nonablated region spectrum might be due to some orientational changes in the crystal structure in the areas in the proximity of the ablated region, which leads to a mixture of Raman spectra corresponding to different scattering geometries [28]. Thus, ultrafast laser ablation clearly induces a permanent local micrometric stress in (Yb,Nb):RTP, as has been reported for such others materials as Nd:MgO:$LiNbO_3$ [28] or Si wafers [29]. This permanent induced stress may be due to the shock waves produced after the absorption of the femtosecond pulse.

Apart from the different intensity observed for these two peaks in the ablated and unablated regions, which is the most evident change in the Raman spectra, the intensity of other peaks also changes. For instance, the intensity of the peak at 976 cm^{-1} is also reduced in the ablated areas. This peak corresponds to the ν_1 vibration of PO_4 tetrahedra [27] indicating that not only are modes related to the TiO_6 group affected by the constraint on their vibrational degrees of freedom, but modes related to PO_4 tetrahedra also are. In fact, the peaks related to Rb-O polar vibration [27] appearing at around 330 cm^{-1} are also affected by the decrease in intensity depending on the polarization analyzed in the spectra, indicating that the whole structure of (Yb,Nb):RTP crystal is affected by the permanent induced stress generated by ultrafast laser ablation.

By comparing the Raman scattering spectra recorded in an area far from the microstructured channel with spectra recorded from ablated grooves and close boundaries, we obtained some information about the dimensions of the affected area during the ablation process. In fact, we found that after ablation, the stressed area up to the groove wall was 3 μm long, as the inset of Fig. 4 shows.

Regarding the depth of the laser affected region, it is worth noting that given the laser repetition rate used for structuring, and the thermal properties of the material ($D = 0.015$ cm^2·s^{-1}), no heat accumulation effects are expected for consecutive pulses [30] during the structuring process. A crude estimation of the heat diffusion length ($L = 2\sqrt{Dt}$) during the absorption of a single pulse leads to a value of $\sim$0.8 nm, much shorter than thickness of the stressed regions. Still, even when a large proportion of the energy of the incoming pulses is expected to be carried with the ablating plasma [31], the material remaining underneath the ablating region is heated by the plasma over much longer time scales and may eventually melt. Ben-Yakar *et al.* [32] provide an expression to estimate the maximum expected thickness of the induced molten using the threshold fluence for ablation and different thermo-optical parameters of the material. Such an estimate leads in our case to a value of $\sim$420 nm for the initial molten layer and a maximum propagated molten layer depth always below than 1 μm. The extension of the stressed region (also not amorphized) seems to be thus more related to the effect of the produced shock waves than to the plasma induced heating of the layer underneath the ablating region.

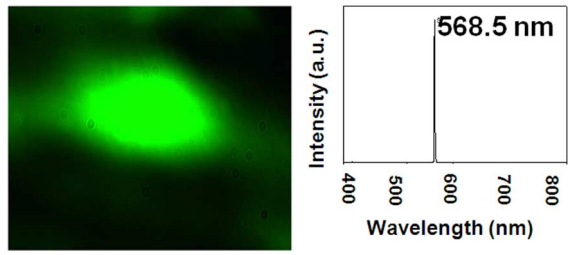

Fig. 5. CCD image of 568.5 nm green light from type II SHG of 1137 nm IR light and the spectra recorded at the end of waveguide.

D. Second Harmonic Generation

A tunable OPO was used to generate radiation with the wavelength required to obtain efficient SHG. The maximum SHG efficiency was obtained pumping with a fundamental beam of 1137 nm of wavelength. The modes excited to produce the green light correspond to a channel waveguide parallel to the $\boldsymbol{a}$ crystallographic direction. They were excited using a microscope objective with the same guiding setup indicated above; an achromatic half-wave plate was placed between the laser source and the sample in order to ensure type II SHG. In fact, the green light generation by type II regime requires guided photons with perpendicular polarizations simultaneously. The guided green light obtained by SHG was recorded with a CCD camera and can be seen in Fig. 5 together with the spectra recorded at the end of the waveguide.

IV. Conclusion

We have produced by fs-laser structuring rib waveguides in (Yb,Nb):RTP/RTP active layers using a combination of approximation scanning and beam multiplexing. The sides of the rib waveguides show a roughness of the order of 500 nm, leading to propagation losses with an upper bound of $\sim$4 dB/cm. This value is lower or comparable to propagation losses before reported with fs-laser structuring in other studies. The approximation used (approximation scanning plus beam multiplexing) has the additional advantage of allowing to produce structures with easily controllable shape in a single scan by controlling the transverse separation of the writing laser spots in the surface.

Taking into account the refractive indexes of the epitaxy and the substrate, as well as the designed geometries, a previous simulation revealed that the confinement can be high. After fs-laser ablation, the simulation with real geometry parameters revealed

that high confinements were still obtained. The near-field pattern of the fundamental mode was observed at 632 and 972 nm, which showed that the guiding was of good quality. Raman spectroscopy reveal some damage to the crystalline structure boundaries in the rib waveguides. This damage was most probably produced by the fs-laser pulses. It is though remarkable that amorphization is not observed. The Raman study showed that the damage boundary region was around 3 μm in length, which is shorter than the total width of the ribs. However, this boundary damage could increase the confinement by increasing the refractive indexes in this zone.

REFERENCES

[1] P. A. Thomas, S. C. Mayo, and B. E. Watts, "Crystal structures of $RbTiOAsO_4$, $KTiO(P_{0.58},As_{0.42})O_4$, $RbTiOPO_4$ and $(Rb_{0.465},K_{0.535})TiOPO_4$, and analysis of pseudosymmetry in crystals of the $KTiOPO_4$ family," *Acta Crystallogr., Sect. B: Struct. Sci.*, vol. B48, pp. 401–407, 1992.

[2] Y. Guillen, B. Ménaert, J. P. Fève, P. Segonds, J. Douady, B. Boulanger, and O. Pacaud, "Crystal growth and refined Sellmeier equations over the complete transparency range of $RbTiOPO_4$," *Opt. Mater.*, vol. 22, pp. 155–162, 2003.

[3] M. N. Satyanarayan, A. Deepthy, and H. L. Bhat, "Potassium titanyl phosphate and its isomorphs: Growth, properties, and application," *Crit. Rev. Solid State Mater. Sci.*, vol. 24, no. 2, pp. 103–191, 1999.

[4] R. Solé, V. Nikolov, I. Koseva, P. Peshev, X. Ruiz, C. Zaldo, M. J. Martín, M. Aguiló, and F. Díaz, "Conditions and possibilities for rare-earth doping of $KTiOPO_4$ flux-grown single crystals," *Chem. Mater.*, vol. 9, pp. 2745–2749, 1997.

[5] A. Peña, J. J. Carvajal, J. Massons, J. Gavaldà, F. Díaz, and M. Aguiló, "Yb:Ta:$RbTiOPO_4$, a new strategy to further increase the lanthanide concentration in crystals of the $KTiOPO_4$ family," *Chem. Mater.*, vol. 19, pp. 4069–4076, 2007.

[6] X. Mateos, V. Petrov, A. Peña, J. J. Carvajal, M. Aguiló, F. Díaz, P. Segonds, and B. Boulanger, "Laser operation of Yb^{3+} in the acentric $RbTiOPO_4$ codoped with Nb^{5+}," *Opt. Express*, vol. 32, pp. 1929–1931, 2007.

[7] J. J. Carvajal, R. Solé, J. Gavaldà, J. Massons, M. Aguiló, and F. Díaz, "Crystal growth of $RbTiOPO_4$:Nb: A new nonlinear optical host for rare earth doping," *Cryst. Growth Des.*, vol. 1, no. 6, pp. 479–484, 2001.

[8] X. Mateos, V. Petrov, A. Peña, J. J. Carvajal, M. Aguiló, F. Díaz, P. Seconds, and B. Boulanger, "Laser operation of Yb^{3+} in the acentric $RbTiOPO_4$ codoped with Nb^{5+}," *Opt. Lett.*, vol. 32, no. 13, pp. 1929–1931, 2007.

[9] J. Cugat, R. Solé, M. C. Pujol, J. J. Carvajal, X. Mateos, F. Díaz, and M. Aguiló, "Waveguiding demonstration on Yb:Nb:$RbTiOPO_4$/$RbTiOPO_4$ (001) epitaxies grown by LPE," *Opt. Mater.*,, vol. 32, pp. 1648–1651, 2010.

[10] J. Cugat, R. Solé, J. J. Carvajal, M. C. Pujol, X. Mateos, F. Díaz, and M. Aguiló, "Crystal growth and characterization of $RbTi_{1-x-y}Yb_xNb_yOPO_4$/$RbTiOPO_4$ (001) non-linear optical epitaxial layers," *CrystEngComm.*, vol. 13, pp. 2015–2022, 2011.

[11] J. Cugat, R. Solé, J. J. Carvajal, X. Mateos, M. C. Pujol, J. Massons, F. Díaz, and M. Aguiló, "Efficient type II phase-matching second-harmonic generation in Ba:Yb:Nb:$RbTiOPO_4$/$RbTiOPO_4$ waveguides," *Opt. Lett.*, vol. 36, no. 10, pp. 1881–1883, 2011.

[12] L. Zhang, P. J. Chandler, P. D. Townsnd, and P. A. Thomas, "Helium ion-implanted optical waveguide in $KTiOPO_4$," *Electron. Lett.*, vol. 28, pp. 650–652, 1992.

[13] C. Grivas and W. Eason, "Dielectric binary oxide films as waveguide laser media: A review," *J. Phys.: Condens. Matter.*, vol. 20, pp. 264011–264014, 2008.

[14] K. Wang, B. Shi, N. Cue, Y. Zhu, R. Xiao, F. Lu, W. Li, and Y. Liu, "Waveguide laser film in erbium-doped $KTiOPO_4$ by pulsed laser deposition," *Appl. Phys. Lett.*, vol. 73, no. 8, pp. 1020–1022, 1998.

[15] W. Bolaños, J. J. Carvajal, X. Mateos, G. S. Murugan, A. Z. Subramanian, J. S. Wilkinson, E. Cantelar, D. Jaque, G. Lifante, M. Aguiló, and F. Díaz, "Mirrorless buried waveguide laser in monoclinic double tungstates fabricated by a novel combination of ion milling and liquid phase epitaxy," *Opt. Express*, vol. 18, pp. 26937–26945, 2010.

[16] F. Laurell, J. Webjörn, G. Arvidsson, and J. Holmberg, "Wet etching of proton-exchanged lithium niobate a novel processing technique," *J. Lightw. Technol.*, vol. 10, no. 11, pp. 1606–1609, 1992.

[17] J. Gottmann, D. Wortmann, I. Vasilief, L. Moiseev, and D. Ganser, "Manufacturing of Nd:$Gd_3Ga_5O_{12}$ ridge waveguide lasers by pulsed laser deposition and ultrafast laser micromachining," *Appl. Surf. Sci.*, vol. 254, pp. 1105–1110, 2007.

[18] R. Solé, V. Nikolov, A. Vilalta, J. J. Carvajal, J. Massons, J. Gavaldà, M. Aguiló, and F. Díaz, "Liquid phase epitaxy of $KTiOPO_4$ on $KTi_{1-x}Ge_xOPO_4$ substrates," *J. Cryst. Growth*, vol. 237, pp. 602–607, 2002.

[19] A. Aznar, O. Silvestre, M. C. Pujol, R. Solé, M. Aguiló, and F. Díaz, "Liquid-phase epitaxy crystal growth of monoclinic $KLu_{1-x}Yb_x(WO_4)_2$/$KLu(WO_4)_2$ layers," *Cryst. Growth Des.*, vol. 6, pp. 1781–1787, 2008.

[20] J. Gottmann, G. Schlaghecken, R. Wagner, and E. W. Kreutz, "Fabrication of erbium-doped planar waveguides by pulsed-laser deposition and laser micromachining," in *Conf. Laser Micromachin. Optoelectron. Device Fabricat. Proc SPIE 4941*, 2003, pp. 148–156, Edited by Ostendorf.

[21] R. D. Leonardo, F. Ianni, and G. Ruocco, "Computer generation of optimal holograms for optical trap arrays," *Opt. Express*, vol. 15, no. 4, pp. 1913–1922, 2007.

[22] B. C. Stuart, M. D. Feit, S. Herman, A. Rubenchik, B. Shore, and M. Perry, "Nanosecond-to-femtosecond laser-induced breakdown in dielectrics," *Phys. Rev.*, vol. B53, pp. 1749–1761, 1996.

[23] A. K. Mairaj, P. Hua, H. N. Rutt, and D. W. Hewak, "Fabrication and characterization of continuous wave direct UV ($\lambda = 244$ nm) written channel waveguides in chalcogenide (Ga:La:S) glass," *J. Light. Tech.*, vol. 20, pp. 1578–1584, 2002.

[24] Y. Jia, N. Dong, F. Chen, J. R. V. D. Aldana, and S. Zhou, "Ridge waveguide lasers in Nd:GGG crystals produced by swift carbon ion irradiation and femptosecond laser ablation," *Opt. Exp.*, vol. 20, pp. 9763–9768, 2012.

[25] G. E. Kugel, F. Bréhat, B. Wyncke, M. D. Fontana, G. Marnier, C. Carabatos-Nedelec, and J. Mangin, "The vibrational spectrum of a $KTiOPO_4$ single crystals studied by Raman and infrared reflectivity spectroscopy," *J. Phys. C: Solid State Phys.*, vol. 21, pp. 5565–5568, 1988.

[26] C. D. Deshpande, A. P. Malshe, E. A. Stach, V. Radmilovic, D. Alexander, D. Doerr, and D. Hirt, "Investigation of femtosecond laser assisted nano and microscale modifications in lithium niobate," *J. Appl. Phys.*, vol. 97, pp. 74316–74325, 2005.

[27] J. J. Carvajal, P. Segonds, A. Peña, J. Zaccaro, B. Boulanger, F. Díaz, and M. Aguiló, "Structural and optical properties of $RbTiOPO_4$:Nb crystals," *J. Phys.: Condens. Matter.*, vol. 19, pp. 116214–116317, 2007.

[28] A. Rodenas, J. A. Sanz García, D. Jaque, G. A. Torchia, C. Mendez, I. Arias, L. Roso, and F. Agulló-Rueda, "Optical investigation of femptosecond laser induced microstress in neodynium doped lithium niobate crystals," *J. Appl. Phys.*, vol. 100, pp. 033521–033529, 2006.

[29] M. S. Amer, M. A. El-Ashry, L. R. Dosser, K. E. Hix, J. F. Maguire, and B. Irwin, "Femptosecond versus nanosecond laser machining: Comparison of induced stresses and structural changes in silicon wafers," *Appl. Surf. Sci.*, vol. 162, pp. 162–167, 2005.

[30] S. M. Eaton, H. Zhang, P. R. Herman, F. Yoshino, L. Shah, J. Bovatsek, and A. Arai, "Heat accumulation effects in femtosecond laser-written waveguides with variable repetition rate," *Opt. Express*, vol. 13, pp. 4708–16, 2005.

[31] T. Y. Choi and C. P. Grigoropoulos, "Plasma and ablation dynamics in ultrafast laser processing of crystalline silicon," *J. Appl. Phys.*, vol. 92, pp. 4918–4925, 2002.

[32] A. Ben-Yakar, A. Harkin, J. Ashmore, R. L. Byer, and H. A. Stone, "Thermal and fluid processes of a thin melt zone during femtosecond laser ablation of glass: the formation of rims by single laser pulses," *J. Phys. D: Appl. Phys.*, vol. 40, pp. 1447–1459, 2007.

Author biographies not included by author request due to space constraints.